Development of an Unsteady Aerodynamic Analysis Module for Rotor Comprehensive Analysis Code

Joonbae Lee*, Kwanjung Yee and Sejong Oh*****
Department of Aerospace Engineering, Pusan National University,
Busan, Republic of Korea

Do-Hyung Kim****
Department of Rotor System, Korea Aerospace Research Institute,
Daejeon, Republic of Korea

Abstract

The inherent aeromechanical complexity of a rotor system necessitated the comprehensive analysis code for helicopter rotor system. In the present study, an aerodynamic analysis module has been developed as a part of rotorcraft comprehensive program. Aerodynamic analysis module is largely classified into airload calculation routine and inflow analysis routine. For airload calculation, quasi-steady analysis model is employed based on the blade element method with the correction of unsteady aerodynamic effects. In order to take unsteady effects – body motion effects and dynamic stall – into account, aerodynamic coefficients are corrected by considering Leishman-Beddoes's unsteady model. Various inflow models and vortex wake models are implemented in the aerodynamic module to consider wake induced inflow. Specifically, linear inflow, dynamic inflow, prescribed wake and free wake model are integrated into the present module. The aerodynamic characteristics of each method are compared and validated against available experimental data such as Elliot's induced inflow distribution and sectional normal force coefficients of AH-1G. In order to validate unsteady aerodynamic model, 2-D unsteady model for NACA0012 airfoil is validated against aerodynamic coefficients of McAlister's experimental data.

Key words : Linear Inflow, Dynamic Inflow, Prescribed Wake, Free Wake, Blade Element Method, Unsteady Effect

Introduction

The inherent aeromechanical complexity of a rotor system necessitated the comprehensive analysis which analyzes aeroelastic and vibration considering aerodynamic-structure interactions simultaneously for helicopter rotor system. Hence, various comprehensive codes such as CAMRAD II, FLIGHTLAB, UMARC and HOST for helicopter rotor system have been developed in the United States and Europe since 1960s. In Korea, it is only recently that the research activities are directed toward developing indigenous helicopter comprehensive code. In the present study, an aerodynamic analysis module has been developed as a part of rotorcraft comprehensive program.

---

* Ph.D. Course
** Associate Professor
E-mail : daedalus@pusan.ac.kr Tel : +82-51-510-2481 Fax : +82-51-513-3760
*** Professor
**** Engineering Researcher

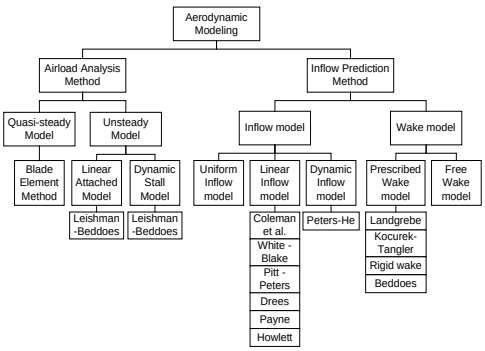

Fig. 1. The structural diagram of aerodynamic module

Fig. 1 shows the structural diagram of aerodynamic analysis module used in this study. Aerodynamic analysis module is largely classified into airload calculation routine and inflow analysis routine. For airload calculation, quasi-steady analysis model is employed based on the blade element method[1] with the correction of unsteady aerodynamic effects. Aerodynamic force and moment coefficients are obtained from look-up tables of 2-D airfoils. In order to take unsteady effects - body motion effects and dynamic stall - into account, aerodynamic coefficients are corrected by considering Leishman-Beddoes's unsteady model[1-3]. Various inflow models and vortex wake models are implemented in the aerodynamic module to consider wake induced inflow. Specifically, linear inflow[1], dynamic inflow[4-5], prescribed wake[1, 6-7] and free wake[8] model are integrated into the present module.

The aerodynamic characteristics of each method are compared and validated against available experimental data such as Elliot[9]'s induced inflow distribution and sectional normal force coefficients of AH-1G[6]. In order to validate unsteady aerodynamic model, 2-D unsteady model for NACA0012 airfoil is validated against aerodynamic coefficients(c_n, c_d, c_m) of McAlister[10]'s experimental data.

Numerical Analysis Methods

The flowchart of aerodynamic module used in this study is illustrated in Fig. 2. At first, an inflow analysis model is selected after calculating initial load under non-induced inflow condition. Next, aerodynamic coefficients are obtained from induced inflow which is calculated by the inflow analysis model and they are corrected by considering unsteady model. Finally, aerodynamic performance given flight condition is obtained by converging C_T. Since the relationship between the rotor aerodynamic parameters(C_T, C_{MX}, C_{MY}) and the blade pitch angles is non-linear, an iterative technique is necessary to obtain the convergence of the trim procedure. A Newton-Raphson iterative method[6] is employed here to trim the rotor automatically.

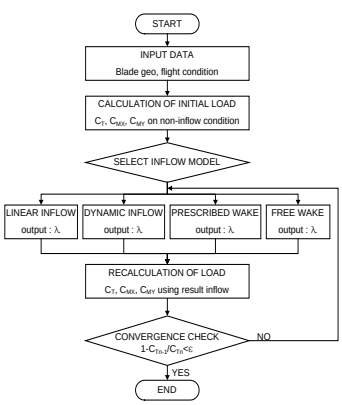

Fig. 2. The flowchart of aerodynamic module

2.1 Quasi-Steady Model

The blade element theory(BET) forms the basis of most modern analyses of helicopter rotor aerodynamics because it provides estimates of the radial and azimuthal distributions of blade aerodynamic loading over the rotor disk. It is necessary to employ unsteady model because it assumes quasi-steady state.

Fig. 3 shows a sketch of the flow environment at representative blade element on the rotor where ϕ is the relative inflow angle. As shown Fig. 3, each velocity component is

$$\frac{U_T}{\Omega R} = r + \mu sin\psi \tag{1}$$

$$\frac{U_P}{\Omega R} = \lambda + \frac{r\dot{\beta}}{\Omega} + \mu\beta cos\psi \tag{2}$$

$$\frac{U_R}{\Omega R} = \mu cos\psi \tag{3}$$

Where μ is the advance ratio, β is the flapping angle and $\dot{\beta}$ is the flapping velocity.

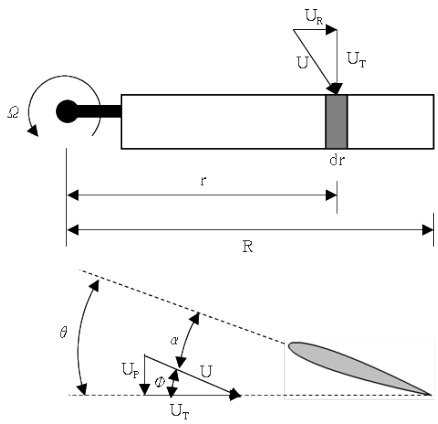

Fig. 3. Aerodynamic environment at a typical blade element

The Aerodynamic parameters are calculated by obtaining aerodynamic force and moment coefficients from look-up tables of 2-D airfoils thorough local effective angle of attack calculated from Eqs. (1)-(3). Furthermore, the Prandtl's tip loss factor is applied to account for three-dimensional effects since the BET assumes that each blade section acts as a quasi-2-D airfoil to produce aerodynamic forces and moments.

2.2 Unsteady Model

In this study, in order to take unsteady effects - body motion effects and dynamic stall - into account, aerodynamic coefficients are corrected by considering Leishman-Beddoes[1-3]'s unsteady model. This aerodynamic model consists of an attached potential flow formulation for linear unsteady airloads, a separated flow formulation for nonlinear unsteady airloads and a dynamic stall formulation for vortex induced airloads. These parts are arranged sequentially such that output from a subsystem forms the input to the next subsystem.

The attached flow formulation is based on the indicial response method in which response is computed from a finite difference approximation to Duhamel's integral[1]. The attached flow solution predicts airloads in a linear attached potential flow regime, under unsteady conditions. In conjunction with the quasi-steady model, this model provides incremental correction factors to the section load parameters. It predicts circulatory and non-circulatory loads separately, and then sums them to attain the final solution.

In general, the indicial normal force and pitching moment response due to step changes in angle of attack and in the pitch rate can be represented by the Eqs. (4)-(7).

$$\frac{C_n(s)}{\alpha} = \frac{4}{M}\phi_\alpha^{nc}(s,M) + C_{l_\alpha}\phi_\alpha^c(s,M) \tag{4}$$

$$\frac{C_m(s)}{\alpha} = -\frac{1}{M}\phi_{\alpha_m}^{nc}(s,M) + C_{l_\alpha}\phi_\alpha^c(s,M)(0.25 - x_{ac}) \tag{5}$$

$$\frac{C_n(s)}{q} = \frac{1}{M}\phi_q^{nc}(s,M) + 2C_{l_\alpha}\phi_q^c(s,M) \tag{6}$$

$$\frac{C_m(s)}{q} = -\frac{7}{12M}\phi_{q_m}^{nc}(s,M) - \frac{C_{l_\alpha}}{4}\phi_{q_m}^c(s,M) \tag{7}$$

The dynamic stall formulation accounts for the vortex induced aerodynamic loads. The formulation models the separation of the concentrated leading edge vortex, its passage over the airfoil chord, and its eventual dissipation into the airfoil wake. Numerically, this is expressed as

$$C_{N_{Vn}} = C_{N_{Vn-1}}\, exp\left(-\frac{\Delta s}{T_v}\right) + (C_{Vn} - C_{Vn-1})exp\left(-\frac{\Delta s}{2T_v}\right) \tag{8}$$

Where C_{NV} is the incremental lift due to time history effect of the dynamic stall, and C_V is the instantaneous excess lift due to the vortex. The T_V is a Mach dependent parameter and is insensitive to airfoil shape.

2.3 Inflow Model

Inflow model is mainly using test data or modeling based on accelerated potential equation. Inflow model is classified into linear model and non-linear model. Linear inflow model include Coleman, Drees, Payne, White-Blake, Pitt-Peters and Howlett model and non-linear inflow model include Peters-He which is generally used to many comprehensive program such as CAMRAD II and FLIGHTLAB.

The longitudinal inflow variation of linear inflow model was determined to be approximately linear. In higher speed forward flight($\mu \geq 0.15$), the time-averaged longitudinal inflow becomes more linear and can be approximately represented by the variation.

$$\lambda_i = \lambda_0\left(1 + k_x\frac{x}{R} + k_y\frac{y}{R}\right) \tag{9}$$

Here k_x and k_y can be viewed as weighting factors. Linear inflow model is classified into several models which are summarized in Table 1. Overall, the Drees, Payne, Pitt-Peters models are found to give the best representation of the inflow gradient as functions of the wake skew angle and the advance ratio when compared to the experimental evidence[1].

Where χ is wake skew angle and μ is advance ratio. In this study, the induced inflow is compared applying Drees model because k_y factor is not zero.

Table 1. Various linear inflow model

	k_x	k_y
Drees	$(4/3)(1-\cos\chi-1.8\mu^2)/\sin\chi$	-2μ
Payne	$(4/3)[(\mu/\lambda)/(1.2+\mu/\lambda)]$	0
Pitt-Peters	$(15\pi/23)\tan(\chi/2)$	0

Peters-He's dynamic inflow model is intermediate-level wake model for inflow analysis of forward flight. The induced inflow distribution can be extended Eq. (10) using parameters for inflow characteristics.

$$\omega(\bar{r},\Psi,\bar{t}) = \sum_{m=0}^{\cdot}\sum_{n=m+1,m+3,\cdots}^{\cdot}\phi_j^r(\bar{r}) \times [\alpha_n^m(\bar{t})\cos(r\Psi) + \beta_n^m(\bar{t})\sin(r\Psi)] \quad (10)$$

The pressure distribution at the rotor disk is expressed in terms of the discrete loading on each moving blade, therefore yielding the effect of a finite number of blades. The explanation for free wake model is illustrated previous study[4-5].

2.4 Wake Model

During the transition from hover into level forward flight, that is, within the range 0.0 $\leq \mu \leq$ 0.1, the induced velocity in plane of the rotor is the most non-uniform, it being strongly affected by the presence of discrete tip vortices that sweep downstream near the rotor plane[1]. In order to overcome this limit, various wake capturing methods such as vortex wake and computational fluid method have developed. The vortex wake method includes prescribed wake and free wake model.

Beddoes's generalized wake model among prescribed wake model is implemented in the aerodynamic module. Since each blade is trailing concentrated vortex lines from a single radial station, then the bound vorticity should be constant along each blade. Since no inboard trailing vortex line is included, the bound vorticity should be constant from the center of the rotor to the contracted radius[7].

The tip vortex strength is obtained from the relationship between thrust and vortex strength of each azimuth angle

$$dT = N_b dL = N_b \rho U d\Gamma \quad (11)$$

Hence, the tip vortex strength from Eq. (12) may be approximated as

$$\Gamma(\psi) = 2\Omega Rc\left(\frac{C_T}{\sigma}\right) \quad (12)$$

The tip vortex strength per 1 rev. is applied periodic function to entire wake filaments.

The induced inflow is calculated by Biot-Savart integration using given tip vortex strength and wake geometry after determining wake geometry by C_T.

Time marching free wake model is integrated into the present module. Vortex wake is calculated by modeling distribution of vortex rings. The induced inflow is calculated using Biot-Savart formula. In addition, Vatistas's vortex-core model[11] is used to resolve the singularity at the center of the vortex. In order to artificially add the viscous diffusion effect on the vortex, Squire's vortex-core growth model[12] is used as follows:

$$r_c(\zeta) = \sqrt{r_{initial}^2 + 4\alpha\delta\nu\zeta/\Omega} \quad (13)$$

Where, $<\alpha=1.25643>$ is the Lamb-Oseen constant, and δ is the average effective viscosity coefficient. In this study, the initial radius of the vortex core is set to be 10% of the blade chord. The explanation for free wake model is illustrated previous study[8].

Results

3.1 Induced Inflow Validation

To understand the inflow characteristics of each method, the longitudinal and lateral induced inflow distributions of each model such as linear inflow, dynamic inflow, prescribed wake, free wake model were compared about advance ratio 0.15 of experimental data of Elliot[9]. The trim angles converged by Newton-Raphson method are compared in Table 2.

As shown Table 2, each model has converged within 1° comparing experimental results. Prescribed wake model's θ_0 value was slightly under predicted but other models θ_0 were over predicted. It can be concluded prescribed wake model's induced inflow is under predicted than other model's induced inflow, since all models have the same thrust.

Longitudinal and lateral inflow distributions are illustrated in Fig. 4. Longitudinal distribution of linear inflow model shows similar gradient compared with experimental results. But lateral distribution of linear inflow model could not predict inflow's non-uniform but predict linear distribution. Dynamic inflow model effectively predicts the trend and has a close correlation with experimental data. It was considered that induced inflow at trailing edge of the longitudinal result was over predicted by tip loss. Prescribed wake model predicts the trend. Induced inflow at trailing edge of the longitudinal distribution was under predicted than experimental data. For lateral distribution of induced inflow, the theoretical prediction agrees well with the variation of experimental results. Free wake model effectively predicts the trend and has a close correlation with experimental data at the longitudinal distribution. But it was similar to He's result near root region.

Linear inflow model has limit to represent non-uniform of induced inflow. Although dynamic inflow model analyze to applying 33 flow states which is equal to He's numerical analysis, inflow difference is shown. This error would be considered difference by airload calculation between He's analysis and present analysis. Free wake model represents induced inflow similar to He's result. Induced inflow at 50% radial station of leading edge was shown error, because wake geometry was fixed by C_T and tip vortex strength was given periodic function in the prescribed wake model. Reasonable results within the theoretical limit about each model could be obtained.

Table 2. Trim angle comparison

	θ_0(°)	θ_{1c}(°)	θ_{1s}(°)
Experiment[9]	6.26	2.08	−1.96
C. He's result[4]	6.86	1.96	−2.26
Linear inflow	6.60	1.60	−2.76
Dynamic inflow	6.84	1.99	−2.35
Prescribed wake	5.76	1.70	−2.08
Free wake	6.38	1.84	−2.23

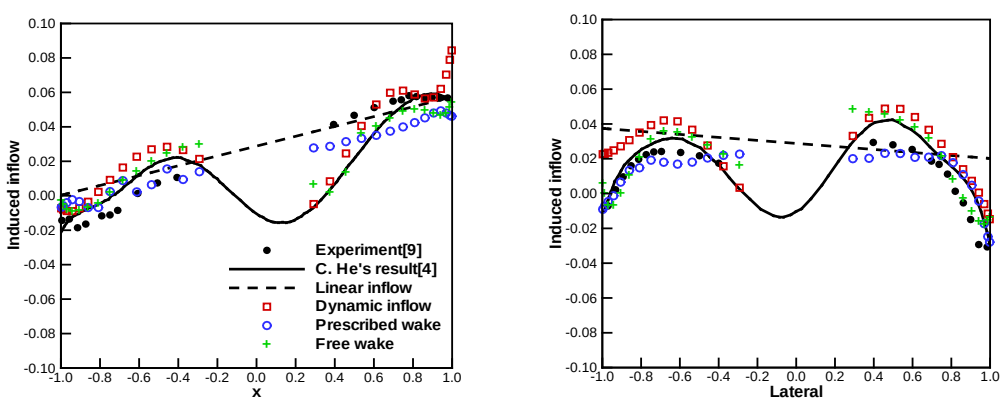

(a) Longitudinal (b) Lateral

Fig. 4. Induced inflow distributions

3.2 Aerodynamic Coefficient Validation

To understand the aerodynamic characteristics of each method, the sectional normal force coefficient and local effective angle of attack of each model were compared about experimental data of AH-1G[6]. In case of sectional normal force coefficient, smooth curve distribution is predicted since inflow model is unable to predict Blade Vortex Interaction(BVI). The trim angles converged by Newton-Raphson method are compared in Table 3. Flapping angle was fixed as β_{1c}=2.13° , β_{1s}=-0.15° .

As shown Table 3, each model has converged within 1° comparing experimental results. Only θ_{1c} value of free wake model represents error more than 1° , collective pitch angle from longitudinal is similar to other models.

Table 3. Trim angle comparison

	θ_0(°)	θ_{1c}(°)	θ_{1s}(°)
Experiment[6]	6.0	1.7	-5.5
Yang[6]	8.0	2.5	-6.5
Linear inflow	5.62	0.64	-4.84
Dynamic inflow	6.65	1.00	-5.23
Prescribed wake	5.62	0.73	-4.67
Free wake	5.87	0.49	-5.00

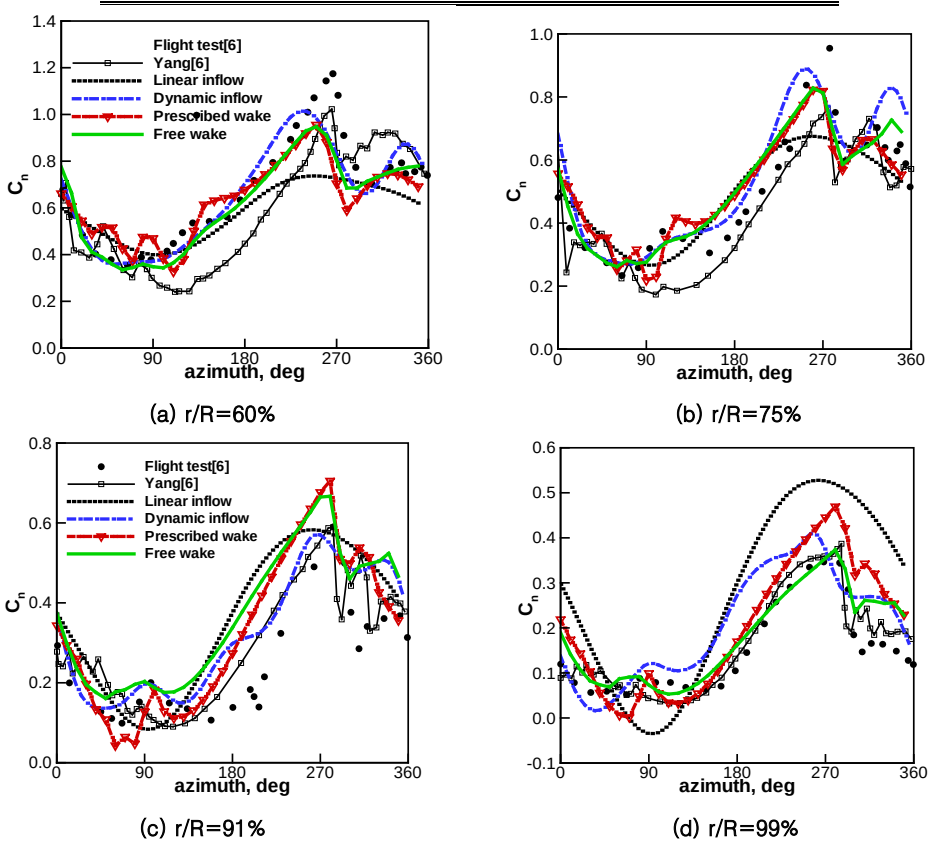

Fig. 5. Sectional normal force coefficient

Fig. 5 shows sectional normal force coefficient with radial position. With like prediction, inflow models illustrated smooth curve distribution. Linear inflow model represents variation like periodic function. Dynamic inflow model described non-uniform of inflow variation well, but error comparing experimental data was shown. At the retreating side near 270° of two wake models, rapid variations due to blade vortex interactions could be seen.

(a), (b) show the results from radial position 60% and 75%. The peak values of all models were predicted lower than experimental data but more approximate than Yang's result. The results of dynamic inflow model were similar to experimental results at advancing side, some error was found at retreating side. This is considered that the induced inflow is calculated equation by flow state. The variation of two wake models is similar to each other. The results are similar to experimental data except for predicting lowly the peak value.

(c), (d) show the results from radial position 91% and 99%. The results of dynamic inflow model were similar to experimental results at advancing side, phase difference about 20° more than other models was found at retreating side. It was considered the theoretical limit of dynamic inflow model. At radial position 91%, peak of wake models was predicted higher than experimental data. It was considered the theoretical limit by method calculating tip vortex strength and error by interpolation of aerodynamic data. Since several significant effects such as the influence of the fuselage, hub and blade elastic deformations were neglected, phase difference was represented[6].

Fig. 6 shows local effective angle of attack of rotor disk. At retreating side near 240° and 50% of radial location, the peak of each model was predicted. Near 300° of linear inflow model, locally peak area was not predicted by induced inflow model. Although induced inflow distribution calculated from method predicting induced inflow of each model was not the same, the local effective angle of attack was similar to each other by controlling trim angle in order to obtain the same thrust. At advancing side near blade tip of prescribed wake model, the distribution due to vortex strength was different from other models. It was considered by theoretical limit of prescribed wake model.

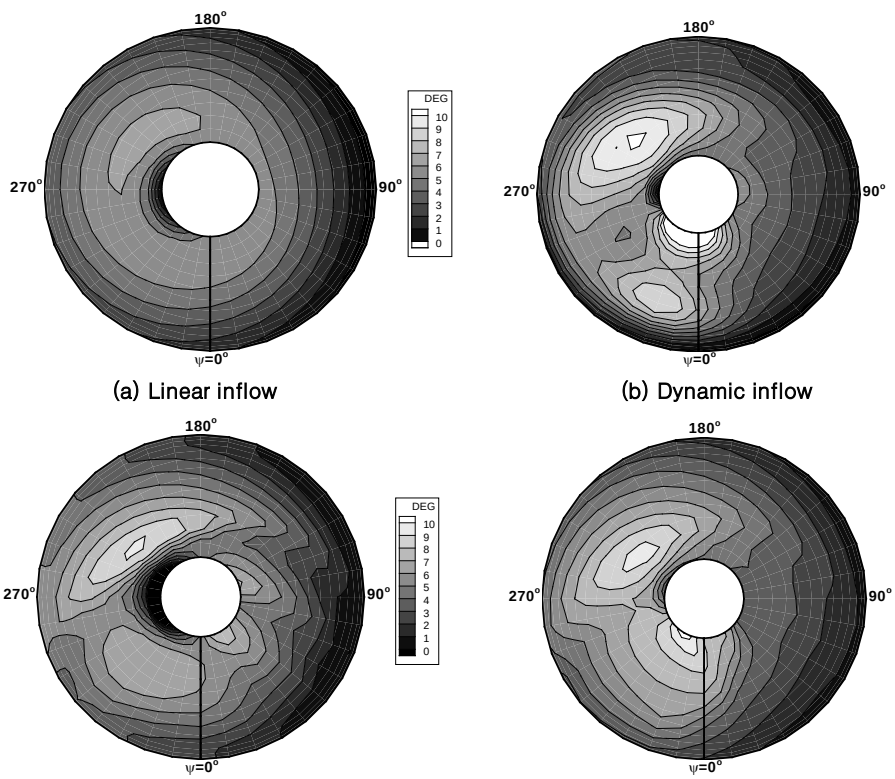

Fig. 6. Effective angle of attack distributions

3.3 Unsteady Analysis Validation

In order to validate Leishman–Beddoes's unsteady aerodynamic analysis model, the aerodynamic coefficients for NACA0012 were compared with McAlister's experimental data. The validating case was shown Table 4.

Table 4. Validation case

	CASE 1	CASE 2
AoA	$10.3° + 8.1°\sin\omega t$	$7.8° + 8.4°\sin\omega t$
M	0.4	0.5
K	0.075	0.06

Where M is Mach number and k is reduced frequency.

$$k = \frac{\omega c}{2V} \tag{14}$$

The unsteady effect was implemented that the reduced frequency calculated by Eq. (14) was larger than 0.05[1]. The case 1 was under unsteady effect field since the reduced frequency of the case 1 was 0.075. The case 2 was predicted weak unsteady effect relatively.

Fig. 7 and shows c_n, c_d and c_m variation along with angle of attack. As shown (a), c_n was increased instantaneously by dynamic stall at near static stall angle. The maximum lift and minimum moment are predicted accurately along with the phasing of the loads during stall. Although some errors have been observed in reattachment, they still show meaningful results for physical phenomenon by dynamic stall. In addition, observed errors are considered by parameters for reattachment, since the dynamic stall model is calculated from many experiential parameters.

Likewise, Fig 8 also shows c_n, c_d and c_m variation along with angle of attack. As shown (a), c_n was increased instantaneously by dynamic stall at near static stall angle. The maximum lift, drag and minimum moment are predicted accurately along with the phasing of the loads during stall. As in Fig. 7, some errors have been observed in reattachment. The errors were also considered by experiential parameters for reattachment.

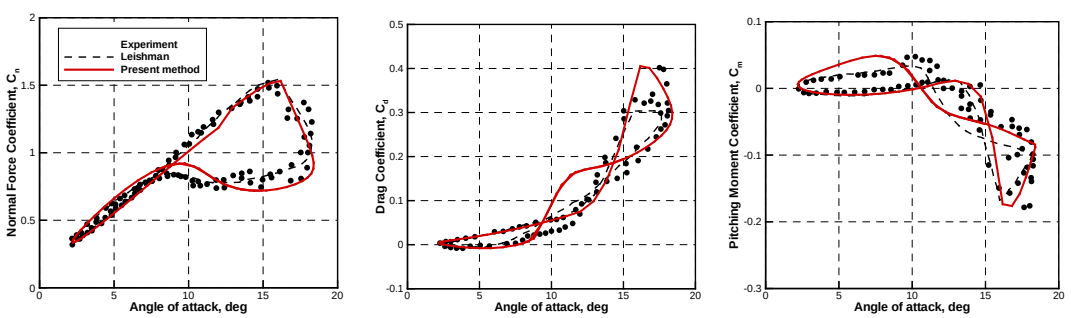

(a) Normal force coefficient (b) Drag coefficient (c) Pitching moment coefficient

Fig. 7. 2–D unsteady effect for NACA0012(CASE 1)

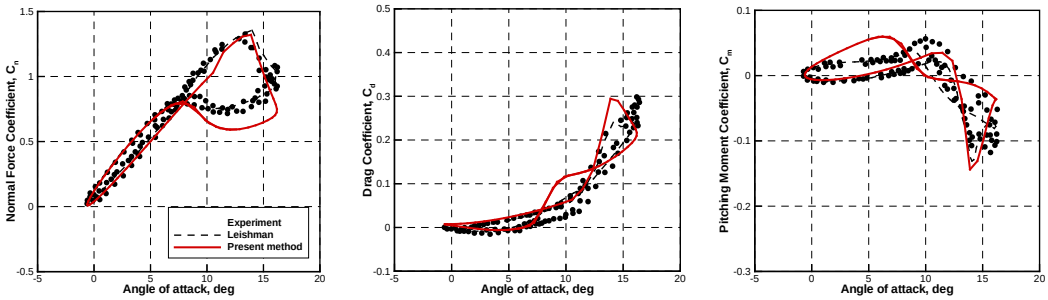

(a) Normal force coefficient (b) Drag coefficient (c) Pitching moment coefficient

Fig. 8. 2-D unsteady effect for NACA0012(CASE 2)

Conclusions

In order to develop present comprehensive program, the aerodynamic analysis module was developed and validated in this study. The aerodynamic characteristics of each method are compared and validated against available experimental data such as Elliot's induced inflow distribution and sectional normal force coefficients of AH-1G.

· Linear Inflow Model

The induced inflow was shown similar gradient compared with experimental data. But the model has theoretical limit to modeling non-uniform of inflow and has low accuracy because of representing periodic function like sine function.

· Dynamic Inflow Model

The non-uniformed inflow distribution is described and is similar to experimental data. Unlike wake model, sectional normal force coefficient is illustrated smooth curve variation. This model is theoretically limited in that it is unable to predict BVI phenomenon because the induced inflow is calculated equation by flow state.

· Prescribed Wake Model

The results of this model are similar to experimental data, but some errors are observed. Since no inboard trailing vortex line is included, the bound vorticity should be constant from the center of the rotor to the contracted radius. This model has theoretical limit such as wake geometry fixed by C_T and tip vortex strength given by 360° period.

· Free Wake Model

The non-uniformed inflow distribution is described and is similar to experimental data. The results of this model comparing with experimental data of AH-1G are the highest accurate than other models.

Although induced inflow distribution calculated by inflow prediction method was not the same, the local effective angle of attack was similar to each other by controlling trim angle in order to obtain the same thrust. The unsteady aerodynamic model about 2-D airfoil shows errors at flow reattachment. Observed errors are considered by parameters for reattachment, since the dynamic stall model is calculated from many experiential parameters.

The distribution and value of each model are different from each other. It was found that the aerodynamic module could yield reasonable results within theoretical limits of each method.

Then, 3-D unsteady aerodynamic model extended from 2-D unsteady model is necessary to validate by comparing with experimental data and analysis results of other comprehensive program.

Acknowledgments

This study has been supported by the KARI under KHP Dual-Use Component Development Program funded by MKE.

References

1. J. G. Leishman, "Principle of Helicopter Aerodynamics 2nd Edition", Cambridge University Press, 2006.

2. J. G. Leishman, T. S. Beddoes, "A Generalized Model for Airfoil Unsteady Aerodynamic Behavior and Dynamic Stall Using the Indicial Method", Proceedings of the 42nd Annual Forum of the American Helicopter Society, Washington D.C., June 1986.

3. G. S. Bir, I. Chopra and et al., "University of Maryland Advanced Rotorcraft Code(UMARC) Theory Manual", Technical Report UM-AERO 94-18, Center for Rotorcraft Education and Research, University of Maryland, College Park, July 1994.

4. C. J. He, "Development and Application of a Generalized Dynamic Wake Theory for Lifting Rotors", Doctor Thesis, Georgia Institute of Technology, 1989.

5. D. A. Peters and C. J. He, "Finite State Induced Flow Models Part II : Three-Dimensional Rotor Disk", Journal of Aircraft, Vol. 32, No. 2, 1995, pp. 323~333.

6. Z. Yang, L. N. Sankar, M. J. Smith and O. Bauchau, "Recent Improvements to a Hybrid Method for Rotors in Forward Flight", Journal of Aircraft, Vol. 39, No. 5, Sep.-Oct., 2002, pp. 804~812.

7. N. M. Komerath and O. A. Schreiber, "Implementation and Validation of a Wake Model for Low-Speed Forward Flight", Final Report, NASA Grant NAG-1-693, Sep., 1987.

8. J. Lee, K. Yee and S. Oh, "Numerical Investigation of Dual Rotors Using a Time-Marching Free-Wake Method", Proc. Of American Helicopter Society 64th Annual Forum, Montreal, Canada, April 29-May 1, 2008.

9. J. W. Elliot, S. L. Althoff and R. H. Sailey, "Inflow Measurement Made with a Laser Velocimeter on a Helicopter Model in Forward Flight- μ =0.15", NASA TM 100541, 1988.

10. K. W. McAlister and L. W. Carr, "Water Tunnel Experiments on an Oscillating Airfoil", NASA TM 78446, 1976.

11. G. H. Vatistas, V. Kozel and W. Mih, "A Simpler Model for Concentrated Vortices", Experiments in Fluids, Vol. 11, 1991, pp. 73~76.

12. H. B. Squire, "The Growth of a Vortex in Turbulent Flow", Aeronautical Quarterly, Vol. 16, Aug. 1965, pp. 302~306.R. C. Baker and B. Charlie, "Nonlinear unstable systems", *International Journal of Control*, Vol. 23, No. 4, 1989, pp. 123~145.